

Dissipation in solids under oscillatory shear: Role of damping scheme and sample thickness

Richard Vink

Institute of Materials Physics, Georg-August-Universität Göttingen, 37073 Göttingen, Germany

(Dated: July 18, 2023)

We study dissipation as a function of sample thickness in solids under global oscillatory shear applied to the top layer of the sample. Two types of damping mechanism are considered: Langevin and Dissipative Particle Dynamics (DPD). In the regime of low driving frequency, and under *strain-controlled* conditions, we observe that for Langevin damping, dissipation *increases* with sample thickness, while for DPD damping, it *decreases*. Under *force-controlled* conditions, dissipation increases with sample thickness for both damping schemes. These results can be physically understood by treating the solid as a one-dimensional harmonic chain in the *quasi-static* limit, for which explicit equations (scaling relations) describing dissipation as a function of chain length (sample thickness) are provided. The consequences of these results, in particular regarding the choice of damping scheme in computer simulations, are discussed.

I. INTRODUCTION

Investigations of dissipative processes by means of (classical) Molecular Dynamics simulations can provide valuable insights at atomic scale resolution. However, the results can be quite ambiguous, since they may depend on the size of the sample that was simulated, as well as on the details of the damping scheme that was used. Langevin damping is presumably the most commonly used such scheme, whereby each atom experiences a friction force whose magnitude is proportional to its velocity. One immediate practical problem is choosing the Langevin damping parameter, which can significantly affect dissipation [1–3].

However, we emphasize here that Langevin damping is by no means the only choice conceivable, and, depending on the system of interest, might not even be optimal. One issue with Langevin damping is its violation of momentum conservation, as well as a spurious dissipation under global translations of the entire system. In this respect, an interesting alternative is the damping scheme of *dissipative particle dynamics* (DPD) [4], which does not suffer from these shortcomings (except for the problem of having to choose a numerical value of the DPD damping parameter, which still remains). While DPD was originally designed to describe complex fluids, it is nowadays also being used to describe the electron-phonon coupling in metals [5].

In addition to the damping scheme come finite-size effects, which also affect dissipation. In principle, finite-size effects can manifest themselves in experimental samples also, and, as such, are not necessarily artifacts. This obviously requires that the experimental sample be small in at least one dimension, a natural candidate being its thickness. Experiments have indeed established that the friction force, under certain conditions, depends on the thickness of the sample, the so-called *thickness effect*. For layered materials, such as graphene, the usual behavior is that friction decreases with increasing sample thickness [6]. In 3D crystals, where the lattice planes

are strongly bound, the trend appears to be reversed, i.e. friction increases with the sample thickness [2, 7–9]. This assumes that the lower part of the sample is rigidly fixed: For a free-standing substrate (membrane) also the reverse behavior is possible [9], but this scenario is not considered here.

It is the purpose of this paper to demonstrate, for the case of a 3D crystal, how sensitive the dependence of dissipation on sample thickness in computer simulations really is: Depending on damping scheme and driving details, both increasing and decreasing behaviors are possible. This shows that great care must be taken when comparing thickness effects in simulations to real experiments. Essentially, the assumptions of the simulation, including the damping scheme, must be argued to resemble experimental conditions. These difficulties already arise in relatively simple situations, for example *low-frequency* and *small-amplitude* oscillatory shear, applied to the top layer of the crystal. Already here, the dissipated energy can be increasing or decreasing with the sample thickness, depending on details.

The physical origin of these different behaviors can be quite easily understood from the simple picture of a driven one-dimensional (1D) bead-spring chain, with which we begin our paper. We consider Langevin and DPD damping schemes, and distinguish between strain- and force-controlled driving scenarios. Next, we verify the 1D findings for a 3D system. In addition, some guidelines are provided as to how one could choose the numerical value of the damping parameters.

II. 1D CHAIN: SCALING LAWS

To understand how dissipation under oscillatory shear depends on the thickness of the sample, it is instructive to consider a 1D “bead-spring” chain. In this section, we derive “scaling laws” for the dissipation as a function of chain length, in the limit of low driving frequency (or, equivalently, short chain length).

A. Undamped chain

Assume a chain consisting of $i = 0, \dots, N - 1$ beads (i.e. N beads in total) positioned on a straight line, the spacing between the beads being a . Each bead (mass m) is connected to its left and right neighbors by springs (spring constant K). The equation of motion for each bead, retaining only terms linear in the bead displacements, then becomes:

$$m\ddot{u}_i = K(u_{i-1} + u_{i+1} - 2u_i), \quad (1)$$

where $u_i \equiv u_i(t)$ is the transversal displacement (SI-unit [u_i] = m) of bead i at time t . Substituting the plane-wave Ansatz, $u_i \propto e^{i(kia - \omega t)}$, into Eq. (1), with wavenumber $k = 2\pi/\lambda$, wavelength λ , and frequency ω , one easily derives the dispersion relation:

$$\omega = 2\Omega_0 \sin(ak/2), \quad \Omega_0 \equiv \sqrt{K/m}. \quad (2)$$

In the long wavelength limit ($k \rightarrow 0$), the above dispersion implies a speed of sound: $c_0 = \lim_{k \rightarrow 0} \omega/k = a\Omega_0$. For metals, $c_0 \sim 10^3$ m/s and $a \sim \text{\AA}$ implying $\Omega_0 \sim \text{THz}$.

B. Chain with Langevin damping

Consider now a damped chain, with the damping (friction) being proportional to the bead velocity, which is the standard choice in Langevin dynamics. The equation of motion then becomes:

$$m\ddot{u}_i = K(u_{i-1} + u_{i+1} - 2u_i) - m\gamma_L \dot{u}_i, \quad (3)$$

with damping parameter γ_L , whose SI-unit [γ_L] = 1/s, i.e. that of frequency. Substituting as before the plane-wave Ansatz, one can solve for the inverted dispersion relation $k(\omega)$, i.e. wavenumber as a function of frequency. While an analytical expression can be obtained, it is more informative to consider the low-frequency regime:

$$k_L \stackrel{\omega \ll \Omega_0}{\approx} \begin{cases} \frac{\omega}{c_0} + \frac{i\gamma_L}{2c_0} & \gamma_L \ll \omega, \\ \frac{\sqrt{\gamma_L \omega}}{c_0} \left(\frac{1+i}{\sqrt{2}} \right) & \gamma_L \gg \omega, \end{cases} \quad (4)$$

where $i^2 = -1$. The wavenumber is complex, meaning the wave is exponentially damped, and only propagates a finite distance $l_L \sim 1/\text{Im}(k_L)$.

C. Chain with DPD damping

Consider again a damped chain, but this time with the damping of the DPD form [4]. In DPD, the damping depends on the velocity difference between nearby pairs of particles, ‘‘penalizing’’ motion that changes the pair distance (two particles moving toward each other, experience friction forces pointing outward, and *vice versa*; particles moving with the same velocity experience no

friction). The DPD approach was originally designed for fluids, but is beneficial in any situation [5] where linear momentum needs to be conserved (recall that Langevin damping, in contrast, does *not* conserve momentum).

For the 1D chain, defining ‘‘nearby’’ to mean pairs of nearest neighboring beads, the DPD equation of motion becomes:

$$m\ddot{u}_i = K(u_{i-1} + u_{i+1} - 2u_i) + m\gamma_D(\dot{u}_{i-1} + \dot{u}_{i+1} - 2\dot{u}_i), \quad (5)$$

where the DPD damping parameter γ_D also has the unit of frequency. Mathematically, one recognizes the DPD term as the finite-difference expression for the second derivative (curvature) of the velocity profile. Substituting again the plane-wave Ansatz, and taking the limit $\omega \ll \Omega_0$, one obtains the wavenumber:

$$k_D \stackrel{\omega \ll \Omega_0}{\approx} \frac{\omega}{c_0} + \frac{\gamma_D a^2 \omega^2 i}{2c_0^3}. \quad (6)$$

The wavenumber is again complex, meaning the wave is damped, decaying on a length scale $l_D \sim 1/\text{Im}(k_D)$.

D. Dissipation scaling laws: Langevin damping

We now consider the Langevin chain under oscillatory shear driving to determine how the *dissipation*, i.e. the energy lost on average per unit of time, depends on the chain length $L = aN$. To this end, bead $i = N - 1$ on one chain end is driven, while bead $i = 0$ on the other end is held fixed ($u_0 = 0$). Under *strain-controlled* driving, the displacement of the driving bead is prescribed:

$$u_{N-1} = A \sin(\omega t), \quad (7)$$

with ω the driving frequency, and A the strain amplitude. Under *force-controlled* driving, a time-dependent driving force is added to the driving bead:

$$F(t) = F_0 \sin(\omega t), \quad (8)$$

with F_0 the driving force amplitude.

In the limit of low driving frequency ω , the entire chain ‘‘keeps up’’ with the driving, and a *quasi-static* approximation becomes reasonable. In this approximation, the chain is always close to its lowest energy configuration, which here is a straight line, implying a *linear* displacement profile:

$$u_i = A \sin(\omega t) \cdot \frac{i}{N-1}. \quad (9)$$

The total averaged dissipation is then easily calculated. Under *strain-control*, the result is:

$$\begin{aligned} P_L^{\text{sc}} &= \frac{1}{p} \int_0^p dt \sum_{i=0}^{N-1} m\gamma_L \dot{u}_i \cdot \dot{u}_i \\ &= \frac{N(2N-1)}{12(N-1)} \cdot m\gamma_L A^2 \omega^2. \end{aligned} \quad (10)$$

In Eq. (10), the summand is the product of the Langevin damping force and velocity of the i -th bead, which corresponds to power; the total dissipation is the sum over all beads; integrating over one driving period $p = 2\pi/\omega$ yields the average dissipation.

Under *force-control*, Eq. (10) still applies, but with the driving amplitude replaced by $A \rightarrow (N-1)F_0/K$, where K is the spring constant of a single spring (for springs in series, the effective stiffness of the entire chain $K_{\text{eff}} \sim K/N$ [10], and so, for a fixed driving force amplitude F_0 , the strain amplitude increases with N because longer chains are effectively “softer”). The dissipation under force-control thus becomes:

$$P_L^{\text{fc}} = \frac{N(2N-1)(N-1)}{12} \cdot \frac{m\gamma_L F_0^2 \omega^2}{K^2}. \quad (11)$$

E. Dissipation scaling laws: DPD damping

Next, we provide the dissipation scaling laws for the DPD chain, again in the quasi-static approximation, i.e. assuming the linear displacement profile of Eq. (9). In this case, under strain-controlled driving, the dissipation becomes:

$$\begin{aligned} P_D^{\text{sc}} &= \frac{1}{p} \int_0^p dt \gamma_D m (\dot{u}_{N-2} - \dot{u}_{N-1}) \cdot \dot{u}_{N-1} \\ &= \frac{1}{2(N-1)} \cdot m\gamma_D A^2 \omega^2. \end{aligned} \quad (12)$$

In Eq. (12), one recognizes the integrand as the DPD damping force acting on the driven bead ($i = N-1$) multiplied by its velocity, which for a linear profile is the only non-zero contribution. The dissipation decreases with N as an inverse power law, and ultimately vanishes.

Under force-control, one again substitutes $A \rightarrow (N-1)F_0/K$, leading to:

$$P_D^{\text{fc}} = \frac{(N-1)}{2} \cdot \frac{m\gamma_D F_0^2 \omega^2}{K^2}, \quad (13)$$

which *increases* linearly with N . Hence, for DPD damping, the dependence of dissipation on chain length is crucially determined by the driving protocol, and can be increasing (force-control) or decreasing (strain-control).

F. Range of validity

Let us now make more precise under what conditions our *quasi-static* thickness-dissipation relations are expected to hold. In the assumed linear profile of Eq. (9), the beads move in phase, which is only possible if the wavelength λ of the wave induced by the driving into the chain far exceeds the chain length aN . The second condition is that the wave must be able to propagate along the entire chain, meaning that also the decay length l

must exceed the chain length. Expressed mathematically, these conditions imply:

$$\lambda = 2\pi/\text{Re}(k) \gg aN, \quad l \sim 1/\text{Im}(k) \gg aN, \quad (14)$$

with k the wavenumber. For each situation at hand, one must check if Eq. (14) is fulfilled, using the appropriate expression for the wavenumber [Eqs. (4) and (6)].

III. 1D CHAIN: SCALING LAW VERIFICATION

We now present Molecular Dynamics (MD) simulations of the driven 1D chain, to verify the scaling laws (the simulations are performed using standard software tools, see Appendix for details). We choose $a \equiv 1$, $m \equiv 1$, and $\tau = 1/\Omega_0 \equiv 1$ as our units of length, mass, and time, respectively. The driving frequency is set to $\omega = 0.001 \ll \Omega_0$, with unit driving amplitudes $A = F_0 = 1$. We do not include any random thermal forces at this point, so the presented results correspond strictly to zero temperature. In the simulations, the dissipation is taken to be the rate of work done driving the top bead $i = N-1$, which takes the general form:

$$P_{\text{dis}} = \left\langle \tilde{F}(t) \tilde{V}(t) \right\rangle_t, \quad (15)$$

where $\langle \cdot \rangle_t$ denotes a time-average.

In the simulations, P_{dis} is obtained from the trajectory, i.e. the time series of the bead displacements $u_i^{\text{MD}}(t)$ and velocities $\dot{u}_i^{\text{MD}}(t)$, where t is time. Under strain-control, the velocity of the driving bead is prescribed by Eq. (7), implying $\tilde{V}(t) = \dot{u}_{N-1}$, the force being $\tilde{F}(t) = -F_{N-1}^{\text{MD}}$, i.e. the sum of elastic and damping forces exerted on the driving bead as obtained from the trajectory (the minus sign is convention, such that in a dissipative system, $P_{\text{dis}} > 0$). Under force-control, the driving force is prescribed by Eq. (8), $\tilde{F}(t) = F(t)$, with now the velocity of the driving bead $\tilde{V}(t) = \dot{u}_{N-1}^{\text{MD}}$ taken from the trajectory. When collecting the time average, the total simulation duration should span an integer multiple of driving periods, with the first few periods discarded to allow for any initial transients to vanish.

We first consider the Langevin chain using damping parameter $\gamma_L = 1.6 \gg \omega$. Fig. 1(a) shows P_{dis} for strain-controlled driving versus the chain length N , as obtained using MD (dots). Applying now the criteria of Eq. (14) with Eq. (4), our dissipation scaling laws should be valid provided $N < N^* \sim c_0/\sqrt{\gamma_L \omega} \sim 25$. The dashed line shows the scaling law, Eq. (10), which, in the regime where $N < N^*$, correctly captures the data (we emphasize that the dashed line is not a fit, since all the parameters in Eq. (10) are known). For $N > N^*$, the wave induced by the driving is so strongly damped, it no longer is able to reach the other chain end. In this case, adding more beads does not affect the dissipation, and so P_{dis} saturates. Fig. 1(b) shows the result for force-controlled driving, the dashed line here corresponding to Eq. (11),

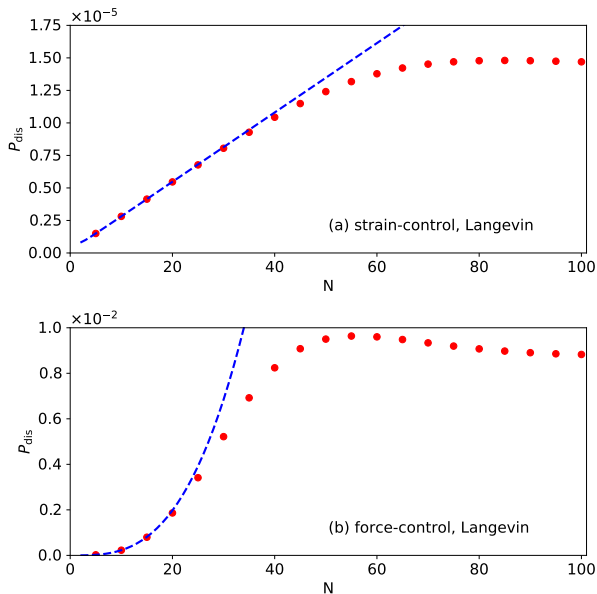


FIG. 1. Dissipation P_{dis} versus chain length N , for the 1D chain with Langevin damping, under (a) strain- and (b) force-controlled driving. The dashed lines show the appropriate asymptotic scaling law, given by Eqs. (10) and (11), respectively.

which, in the regime $N < N^*$, also correctly captures the data.

In Fig. 2, we show the analogous results for the DPD chain, using $\gamma_D = 1.6$. Following Eq. (6), the wave length $\lambda = 2\pi/\text{Re}(k_D) \sim 6300$ and decay length $l_D \sim 1/\text{Im}(k_D) > 10^6$, which both far exceed our considered chain lengths. In line with the criteria of Eq. (14), the DPD scaling laws thus capture the entire data range. Note the pronounced qualitative difference: decreasing dissipation with N for strain-control, increasing for force-control.

IV. DISSIPATION IN A 3D CUBIC CRYSTAL

We now consider a 3D crystal, using essentially the particle model of Ref. [11]. The crystal structure is taken to be *simple-cubic*, the lattice constant $a \equiv 1$ being our unit of length. We use simulation cells of size $N_x = N_y = 20$ in the two lateral directions; the number of vertical layers is denoted N_z . Periodic boundary conditions are applied in the lateral directions, but not in the vertical one. Between nearest- and next-nearest neighboring atoms harmonic bonds are placed, both with spring constant K , the rest-lengths of the springs being 1 and $\sqrt{2}$, respectively, such that the perfect crystal configuration has zero energy. We again take the single particle mass to be unity, $m \equiv 1$, and as unit of time $\tau = 1/\Omega_0 = \sqrt{m/K} \equiv 1$. In these units, the (zero-temperature) shear modulus of the crystal $G = 2$, Young modulus $E = 5$, and Poisson ratio

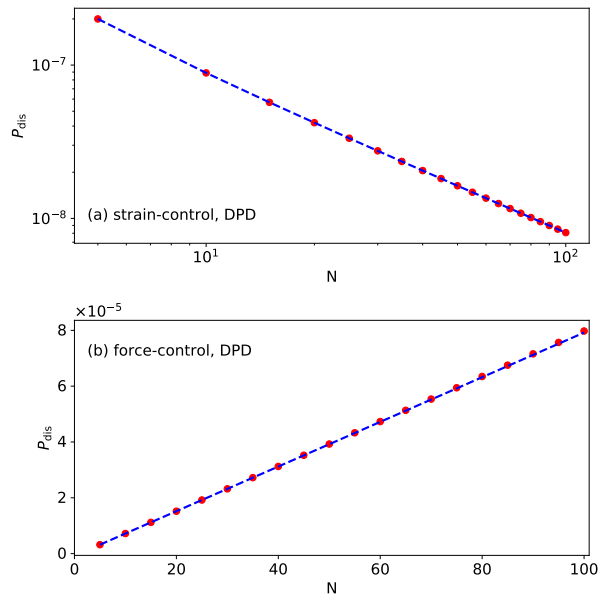


FIG. 2. Analogue of Fig. 1, using DPD damping, with scaling laws given by Eqs. (12) and (13). Note that panel (a) uses double-logarithmic scales.

$\nu = 0.25$ (which were obtained numerically by deforming the crystal cell and energy minimization).

The bottom layer of the crystal is kept fixed, while the top layer is harmonically driven in the x -direction with frequency $\omega = 2\pi \cdot 0.001$, corresponding to a global oscillatory shear deformation. We consider both *strain-* and *force-*controlled scenarios, the respective driving amplitudes being $A = F_0 = 0.05$. For strain-controlled driving, the x -displacement of each atom in the top layer is prescribed, $u_x = A \sin(\omega t)$, with u_x measured from the perfect lattice position (the remaining y, z components are allowed to move freely under the influence of elastic and damping forces). For force-controlled driving, atoms in the top layer have an additional force component in the x -direction, $F_x = F_0 \sin(\omega t)$, added to them. The dynamics of the system is obtained using MD (see Appendix for details). The dissipation is again measured using Eq. (15), but divided by $N_x N_y$, so that the reported dissipation P_{dis} is here to be understood as the dissipation *per surface atom*.

A. Zero temperature

We first consider the crystal with Langevin damping at zero temperature. In 3D, the Langevin damping force acting on particle i is given by $\vec{F}_{L,i} = -m\gamma_L \vec{v}_i$, with \vec{v}_i the velocity *vector* of particle i . With the exception of the frozen bottom layer, the damping force is applied to every particle in the system, including those being driven, using $\gamma_L = 2 \gg \omega$. Following Eqs. (4) and (14), our dissipation scaling laws should hold pro-

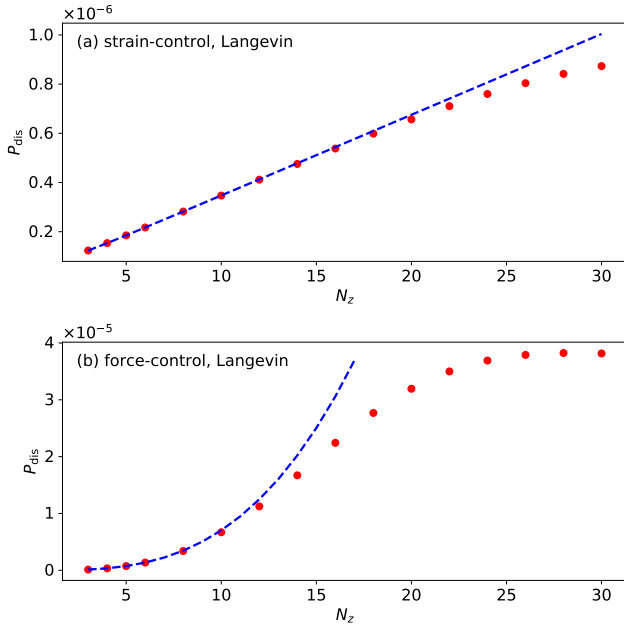


FIG. 3. Dissipation P_{dis} (per surface atom) versus the number of vertical layers N_z , for a 3D cubic crystal with Langevin damping, under (a) strain- and (b) force-controlled driving. Dots show simulation results, dashed lines the appropriate asymptotic scaling law, given by Eqs. (10) and (11), respectively.

vided $N_z < N_z^* \sim 13$. In Fig. 3, we show the dissipation as a function of the number of vertical layers N_z for (a) strain- and (b) force-controlled driving. The dashed lines show Eqs. (10) and (11) with, in the latter, K replaced by the shear modulus G . Again, these lines are not fits, since all the required quantities are known. For small N_z , the agreement is excellent; deviations appear when $N_z \sim N_z^*$, as expected. Our observations imply that each crystal layer effectively moves as a single entity, i.e. can be treated as one massive bead. Since the driving amplitude here is small, only shear motion is induced, the coupling to longitudinal motion being negligible, which explains why the crystal behaves effectively as a 1D chain.

Next, we consider the crystal with DPD damping at zero temperature. The DPD damping force is computed for every bond in the system (nearest- and next-nearest neighbors). The corresponding forces are applied to all particles, including driven ones, but excluding the bottom layer. In 3D, the DPD damping force acting on particle i due to a bonded neighbor j is given by $\vec{F}_{D,i} = m\gamma_D \hat{r}_{ij} \cdot (\vec{v}_j - \vec{v}_i) \hat{r}_{ij}$ [4], with \hat{r}_{ij} the unit vector pointing from particle $i \rightarrow j$ (due to Newton's third law, particle j feels the same force acting in the opposite direction, $\vec{F}_{D,j} = -\vec{F}_{D,i}$). The total damping force on any given particle is obtained by summing over its bonded neighbors (some of which may involve frozen particles of the bottom layer). In Fig. 4, we show the dissipation as a function of the number of vertical layers N_z for (a) strain- and (b) force-controlled driving, using damp-

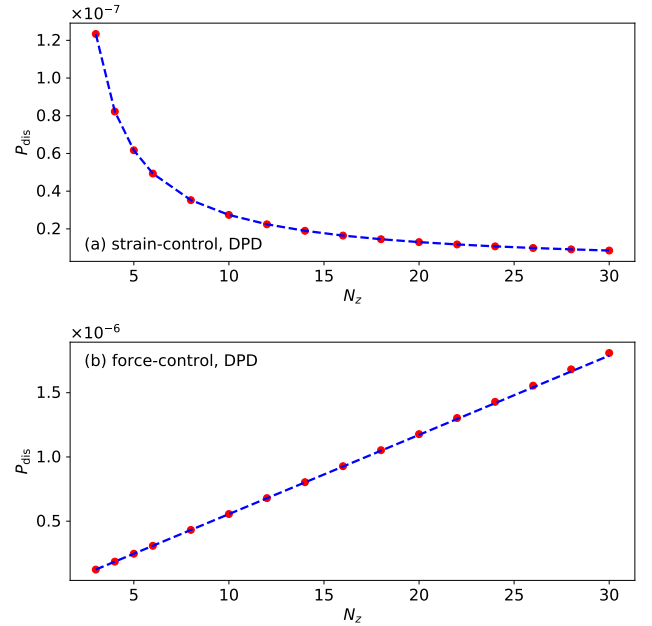


FIG. 4. Analogue of Fig. 3, using DPD damping, with scaling laws given by Eqs. (12) and (13).

ing parameter $\gamma_D = 5$. The dashed lines show Eqs. (12) and (13), with K again replaced by the shear modulus G . Following Eq. (6), one sees that the wavelength and the decay length both far exceed the simulated thicknesses ($\lambda, l_D \gg aN_z$), and so, in line with Eq. (14), the scaling laws capture the full data range. Note again that the dissipation decreases with N_z under strain-control, and that it increases under force-control.

B. Finite temperature

The results presented so far apply to zero temperature, but we expect agreement at finite temperature also, provided one remains in the solid phase. For a typical metal at room temperature, the ratio of thermal to elastic energy $k_B T / m c_0^2 \sim 10^{-3}$ (Boltzmann constant k_B), with c_0 the transversal speed of sound, i.e. elasticity still dominates. To verify, we have repeated two of our MD runs with random thermal forces included, using $k_B T = 0.005$ in our energy units, while keeping all other parameters the same. For the Langevin system, random forces were implemented following Ref. [12]; for DPD, the momentum-conserving noise term of Ref. [4] was used. Results are shown in Fig. 5, using strain-controlled driving, for the Langevin (a) and DPD crystal (b). Provided the simulation spans sufficiently many driving periods, the average dissipation (dots) remains well described by the “ $T = 0$ ” scaling laws. However, there is a sizable thermal fluctuation (error bars) meaning that, for a single cycle, there can be considerable deviations from these laws (by increasing the lateral system size, $N_x N_y \rightarrow \infty$, we expect these fluctuations to vanish though).

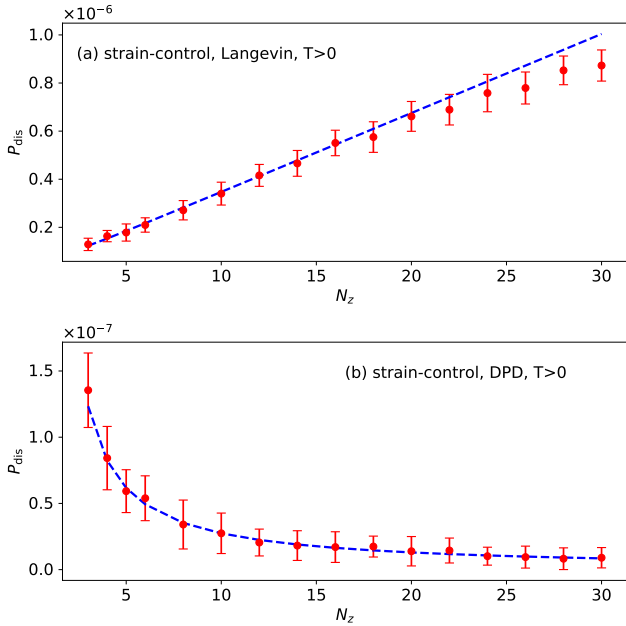


FIG. 5. Numerically obtained dissipation (dots) under strain control for a 3D cubic crystal at *finite temperature* with (a) Langevin and (b) DPD damping versus the number of vertical layers N_z (dots show the dissipation averaged over 50 driving periods; error bars indicate the corresponding standard deviation). The dashed lines show Eqs. (10) and (12), respectively.

V. SUMMARY AND CONCLUSIONS

We studied dissipation in solids subjected to global oscillatory shear as a function of sample thickness. We considered the effect of the damping mechanism (Langevin vs. Dissipative Particle Dynamics) as well as that of the driving protocol (strain- vs. force-controlled). Depending on these, dissipation can either increase or decrease with sample thickness. These findings can be understood physically using the 1D harmonic chain as model to describe the solid. Possible *experimental* verification to determine which damping mechanism is the relevant one, Langevin or DPD, could be performed by measuring the dissipation for various sample thicknesses under global oscillatory shear for a known driving protocol.

Regarding the use of DPD to describe the electron-phonon coupling in metals [5], we still provide the typical value of the damping parameter γ_D that should be used. Based on the number provided in Ref. [5], the DPD damping parameter $\gamma_D \sim \alpha^2/m \sim 1.6$ THz (this uses $\alpha^2 = 0.01$ eV ps/ \AA^2 for Nickel provided in Ref. [5], with m the Nickel atomic mass). It is interesting to see

what attenuation length this number implies. Following Eq. (6) and assuming ultrasound driving ($\omega \sim 10$ MHz), the above value of γ_D , together with $c_0 \sim 3000$ m/s and lattice constant $a = 3.5$ \AA , yield a decay (attenuation) length $l_D \sim 1$ m. This would be the attenuation in a perfect crystalline sample, and with electron-phonon coupling being the only dissipation channel. The actually measured attenuation in real metals in the ultrasound regime is typically ~ 100 dB/m [13], corresponding to an attenuation length of centimeters, i.e. significantly smaller. This shows that, in real metals, other mechanisms (besides electron-phonon coupling) also are at play, enhancing dissipation [14, 15].

We still illustrate a delicate point that arises when damping schemes are used to model real materials, say, for the purpose of MD simulation. As stated before, any such scheme requires that the damping parameter be specified. For Langevin and DPD, these parameters are γ_L and γ_D , respectively. A sensible approach might seem to fit these parameters to the attenuation length. For any given driving frequency and for each damping scheme (Langevin or DPD), one can always select the damping parameter to match a desired attenuation length, using Eqs. (4) and (6). However, the corresponding dissipation between the damping schemes will be very different, see for example Fig. 5, even if the attenuation is the same! In other words, mere agreement with the attenuation length is no guarantee that also the dissipation will be captured correctly. Instead, additional microscopic information is needed to select the appropriate damping model.

ACKNOWLEDGMENTS

This work was supported by the Deutsche Forschungsgemeinschaft (DFG, German Research Foundation) – 217133147/SFB 1073, project A01.

Appendix A: MD Simulation details

The 1D chain simulations were performed by integrating the equations of motion using the Runge-Kutta-Fehlberg method of the GNU Scientific Library [16] with integration timestep $\Delta t = 0.005$. The MD simulations of the 3D crystal were performed with LAMMPS [17] using integration time step $\Delta t = 0.001$. To implement DPD bonds, a custom bond style was coded; all other aspects of the simulations can be modeled with LAMMPS using its standard features.

[1] Richard L. C. Vink, “Connection between sliding friction and phonon lifetimes: Thermostat-induced thermolubricity effects in molecular dynamics simulations,” *Physical*

Review B **100**, 094305 (2019).

[2] A. Benassi, A. Vanossi, G. E. Santoro, and E. Tosatti, “Parameter-free dissipation in simulated sliding friction,”

- Physical Review B **82**, 081401 (2010).
- [3] Dawid Toton, Christian D Lorenz, Nikolaos Rompotis, Natalia Martsinovich, and Lev Kantorovich, “Temperature control in molecular dynamic simulations of non-equilibrium processes,” *Journal of Physics: Condensed Matter* **22**, 074205 (2010).
- [4] P Español and P Warren, “Statistical mechanics of dissipative particle dynamics,” *Europhysics Letters (EPL)* **30**, 191–196 (1995).
- [5] A. Tamm, M. Caro, A. Caro, G. Samolyuk, M. Klintonberg, and A. A. Correa, “Langevin dynamics with spatial correlations as a model for electron-phonon coupling,” *Physical Review Letters* **120**, 185501 (2018).
- [6] David Andersson and Astrid S. de Wijn, “Understanding the friction of atomically thin layered materials,” *Nature Communications* **11** (2020), 10.1038/s41467-019-14239-2.
- [7] Seiji Kajita, Hitoshi Washizu, and Toshihide Ohmori, “Deep bulk atoms in a solid cause friction,” *EPL (Europhysics Letters)* **87**, 66002 (2009).
- [8] Niklas A. Weber, Miru Lee, Florian Schönwald, Leonard Schüler, Vasily Moshnyaga, Matthias Krüger, and Cynthia A. Volkert, “Nanoscale friction controlled by top layer thickness in $[\text{lamno}_3]_m/[\text{srmno}_3]_n$ superlattices,” (2022).
- [9] Miru Lee, Niklas Weber, Cynthia A. Volkert, and Matthias Krüger, “Friction on layered media: How deep do phonons reach?” *Europhysics Letters* **142**, 46001 (2023).
- [10] Liang Xu, Tian-Bao Ma, Yuan-Zhong Hu, and Hui Wang, “Vanishing stick–slip friction in few-layer graphenes: the thickness effect,” *Nanotechnology* **22**, 285708 (2011).
- [11] Miru Lee, Richard L. C. Vink, Cynthia A. Volkert, and Matthias Krüger, “Noncontact friction: Role of phonon damping and its nonuniversality,” *Physical Review B* **104**, 174309 (2021).
- [12] Burkhard Dünweg and Wolfgang Paul, “Brownian Dynamics Simulations Without Gaussian Random Numbers,” *International Journal of Modern Physics C* **02**, 817–827 (1991).
- [13] Kanji Ono, “A comprehensive report on ultrasonic attenuation of engineering materials, including metals, ceramics, polymers, fiber-reinforced composites, wood, and rocks,” *Applied Sciences* **10**, 2230 (2020).
- [14] Kurt Lücke, “Ultrasonic attenuation caused by thermoelastic heat flow,” *Journal of Applied Physics* **27**, 1433–1438 (1956).
- [15] R. Kishore, “Acoustic attenuation in solids,” *Physical Review* **173**, 856–859 (1968).
- [16] M. Galassi *et al.*, *GNU Scientific Library Reference Manual (3rd Ed.)*.
- [17] Aidan P. Thompson, H. Metin Aktulga, Richard Berger, Dan S. Bolintineanu, W. Michael Brown, Paul S. Crozier, Pieter J. in 't Veld, Axel Kohlmeyer, Stan G. Moore, Trung Dac Nguyen, Ray Shan, Mark J. Stevens, Julien Tranchida, Christian Trott, and Steven J. Plimpton, “LAMMPS - a flexible simulation tool for particle-based materials modeling at the atomic, meso, and continuum scales,” *Computer Physics Communications* **271**, 108171 (2022).